

Supplementary Information

Exploring Photooxidative Degradation Pathways of Harmol and Harmalol alkaloids in Water: Effects of pH, Excitation Sources and Atmospheric Conditions

*Fernando D. Villarruel,^a M. Paula Denofrio,^a Tobias Schmidt de León,^{b,c} Rosa Erra-Balsells,^{b,c} Ezequiel Wolcan,^d Fernando S. García Einschlag,^d and Franco M. Cabrerizo^{a, *}*

^a Instituto Tecnológico de Chascomús (INTECH), Universidad Nacional de San Martín (UNSAM) - Consejo Nacional de Investigaciones Científicas y Técnicas (CONICET), Av. Intendente Marino Km 8.2, CC 164 (B7130IWA), Chascomús, Argentina. E-mail: fcabrerizo@intech.gov.ar

^b Universidad de Buenos Aires. Facultad de Ciencias Exactas y Naturales. Departamento de Química Orgánica. Pabellón II, 3er P., Ciudad Universitaria, (1428) Buenos Aires, Argentina.

^c CONICET, Universidad de Buenos Aires. Centro de Investigación en Hidratos de Carbono (CIHIDECAR). Facultad de Ciencias Exactas y Naturales. Pabellón II, 3er P., Ciudad Universitaria, (1428) Buenos Aires, Argentina.

^d Instituto de Investigaciones Fisicoquímicas Teóricas y Aplicadas (INIFTA), CCT-La Plata-CONICET, Universidad Nacional de La Plata, Diag. 113 y 64 (1900), La Plata, Argentina

* To whom correspondence should be addressed (fcabrerizo@intech.gov.ar)

Index

| | |
|--|-----|
| 1. UV-visible spectroscopic analysis of 1C air-equilibrated solutions irradiated (R-350) under different pH conditions | S3 |
| 2. UV-visible spectroscopic analysis of 2C air-equilibrated solutions irradiated (R-350) under different pH conditions | S4 |
| 3. Normalized emission spectra of R-350 and LED-426 | S5 |
| 4. UV-visible spectroscopic analysis of 2C irradiated (LED-426) solution under air-equilibrated and N ₂ -sat conditions | S6 |
| 5. Fluorescence (EEMs) spectroscopic analysis of 1C air-equilibrated solutions irradiated (R-350) under different pH conditions | S7 |
| 6. Fluorescence (EEMs) spectroscopic analysis of 1C N ₂ -sat solutions irradiated (R-350) under acidic (pH 4.2) conditions | S8 |
| 7. Fluorescence (EEMs) spectroscopic analysis of 2C air-equilibrated solutions irradiated (R-350) under different pH conditions | S9 |
| 8. Fluorescence (EEMs) spectroscopic analysis of 2C N ₂ -sat solutions irradiated (R-350) acidic (pH 4.2) conditions | S10 |
| 9. Fluorescence (EEMs) spectroscopic analysis of 2C solutions irradiated (LED-426) under different atmospheres | S11 |
| 10. UV-visible spectroscopic analysis of thermal reaction from 1C irradiated under different pH conditions | S12 |
| 11. UV-visible spectroscopic analysis of thermal reaction from 2C irradiated under different pH conditions | S13 |
| 12. UV-visible spectroscopic analysis of thermal reaction from 2C irradiated with LED-426 atmospheric conditions | S14 |
| 13. UV-visible spectroscopic analysis of thermal reaction from 2C irradiated under different atmospheric conditions | S15 |
| 14. MCR-ALS analysis of 1C irradiated under different pH conditions | S16 |
| 15. MCR-ALS analysis of 2C irradiated under different pH conditions | S17 |
| 16. UV-visible spectroscopic titration of irradiated 1C solutions | S18 |
| 17. MCR-ALS analysis of the thermal reaction of 1C and 2C irradiated solutions under different pHs | S19 |
| 18. ESI analysis of relative intensities of 2C / 1C | S20 |
| 19. TD-DFT calculated electronic transitions and simulated spectra for the cationic (C) and quinonic (Q) species of compounds 1 and 2. | S21 |
| 20. Numerical support for H ₂ O ₂ quantification | S22 |

1. UV-visible spectroscopic analysis of 1C air-equilibrated solutions irradiated (R-350) under different pH conditions

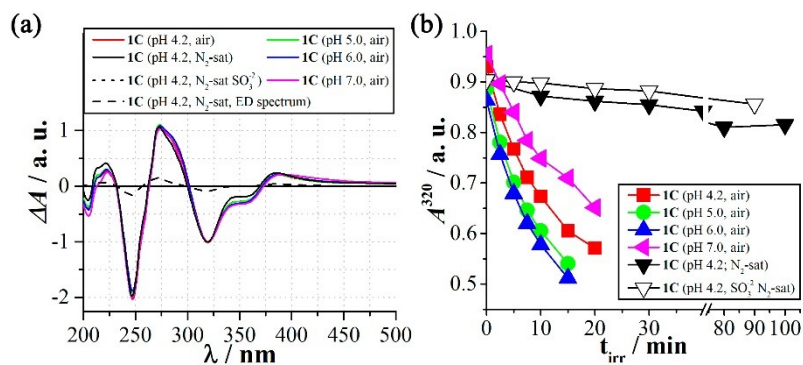


Figure SI.1. (a) and (b) NED_{tirr} spectra and kinetics monitored by UV-vis absorption spectra of aqueous solution of 1C (33 μM), irradiated (R-350) under two different atmospheric conditions (*i.e.*, air-equilibrated and N₂-sat) and three different pHs (5.0, 6.0, and 7.0). With comparative reasons, data presented in the main text corresponding to the pH 4.2 acidic condition are also depicted herein. Sodium sulfite (Na₂SO₃) was also added as scavenger of molecular oxygen to improve the anaerobic conditions.

2. UV-visible spectroscopic analysis of 2C air-equilibrated solutions irradiated (R-350) under different pH conditions

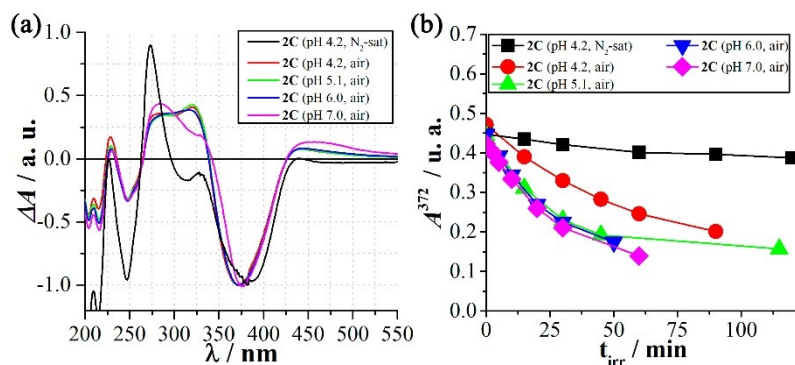


Figure SI.2. (a) and (b) NED_{irr} spectra and kinetics monitored by UV-vis absorption spectra of aqueous solution of 2C (30 μM), irradiated (R-350) under two different atmospheric conditions (*i.e.*, air-equilibrated and N₂-sat) and three different pHs (5.1, 6.0, and 7.0). With comparative reasons, data presented in the main text corresponding to the pH 4.2 acidic condition are also depicted herein.

3. Normalized emission spectra of R-350 and LED-426

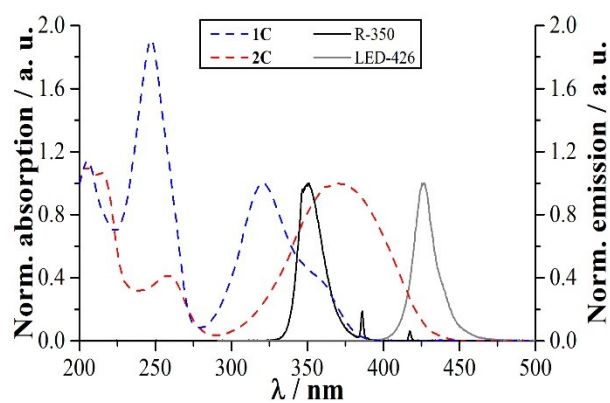


Figure SI.3. Normalized emission spectra of the two different excitation sources (R-350 and LED-426) used in this work.

4. UV-visible spectroscopic analysis of 2C irradiated (LED-426) solution under air-equilibrated and N₂-sat conditions

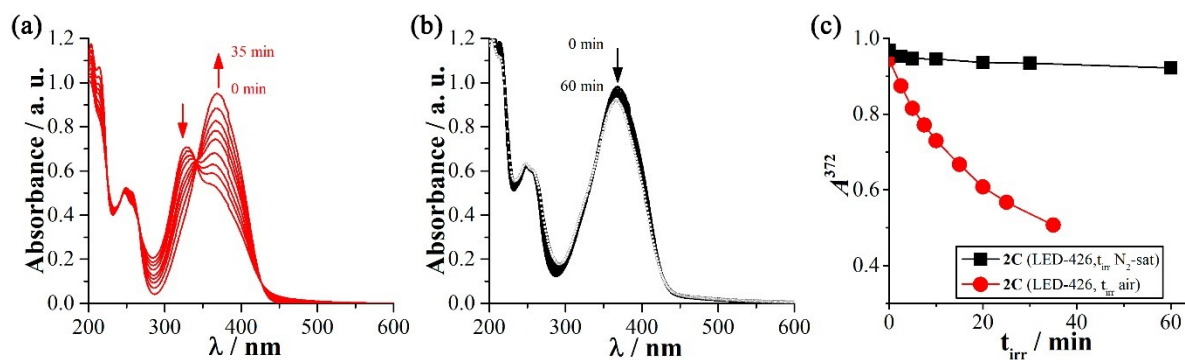


Figure SI.4. (a) y (b) Evolution of the UV-vis absorption spectra of acidic (pH 4.2) aqueous solution of 2C (60 μM) under air-equilibrated and N₂-sat atmospheric conditions, respectively, recorded as a function of the irradiation time with LED-426. Measurements were made using quartz cells of 1 cm optical path lengths. Single spectra depicted in Orange and grey were recorded from 2C irradiates solutions, respectively, storage in the dark during 24 h (thermal reaction). (c) Comparative kinetics showing the evolution of $A^{372\text{nm}}$ of spectra depicted in (a) and (b).

5. Fluorescence (EEMs) spectroscopic analysis of 1C air-equilibrated solutions irradiated (R-350) under different pH conditions

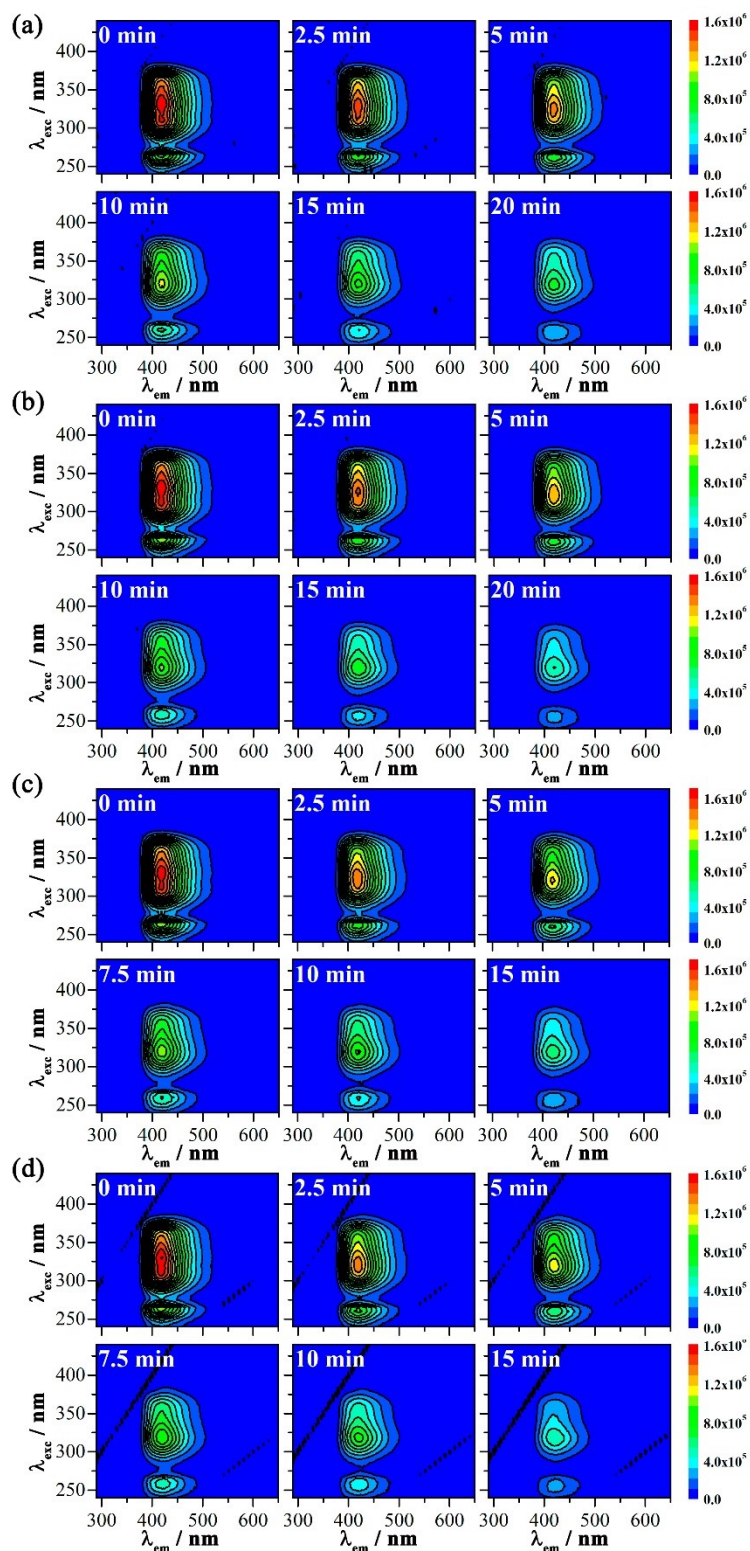


Figure SI.5. EEMs of 1C air-equilibrated solutions irradiated (R-350) under different pHs conditions: (a) 4.2, (b) 5.0, (c) 6.0 and (d) 7.0.

6. Fluorescence (EEMs) spectroscopic analysis of 1C N₂-sat solutions irradiated (R-350) acidic (pH 4.2) conditions

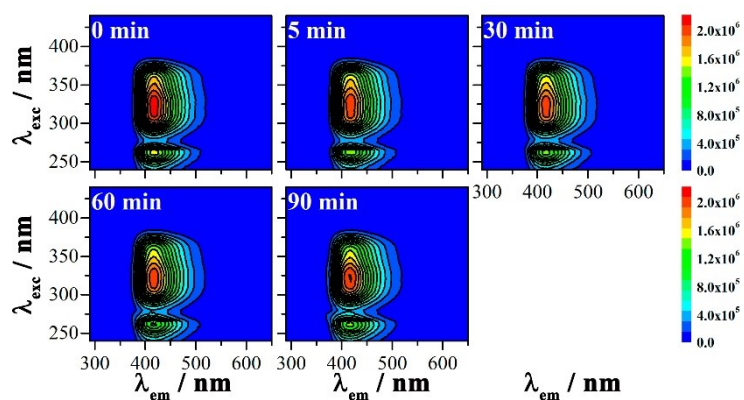


Figure SI.6. EEMs of 1C acidic (pH 4.2) solutions irradiated (R-350) under N₂-sat conditions.

7. Fluorescence (EEMs) spectroscopic analysis of 2C air-equilibrated solutions irradiated (R-350) under different pH conditions

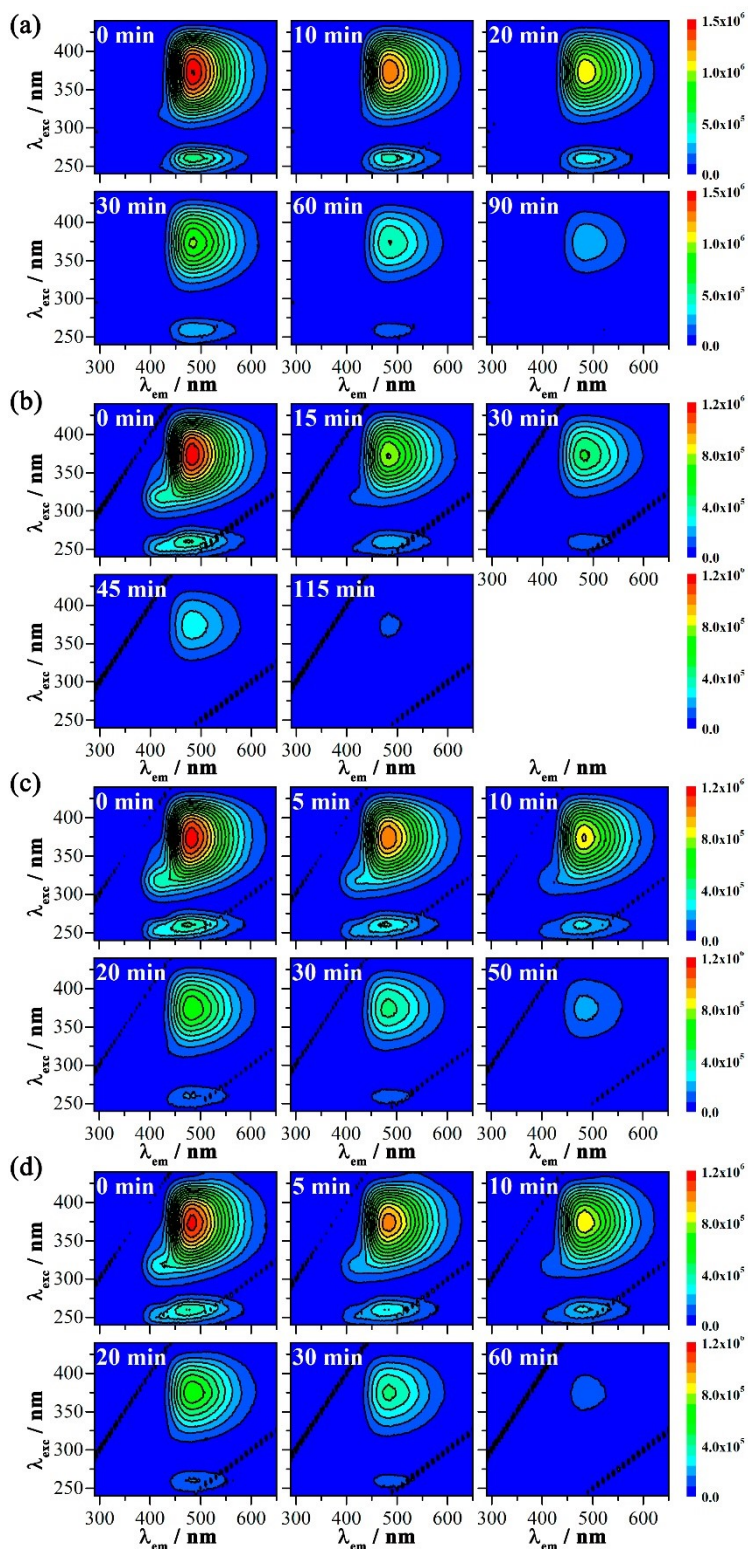


Figure SI.7. EEMs of 2C air-equilibrated solutions irradiated (R-350) under different pHs conditions: (a) 4.2, (b) 5.0, (c) 6.0 and (d) 7.0.

8. Fluorescence (EEMs) spectroscopic analysis of 2C N₂-sat solutions irradiated (R-350) acidic (pH 4.2) conditions

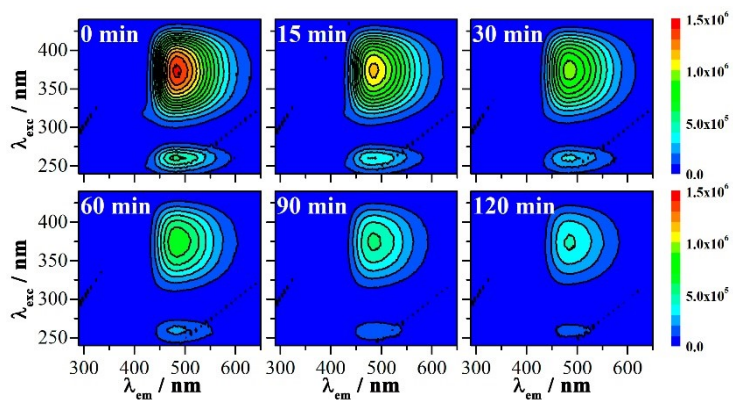


Figure SI.8. EEMs of 2C acidic (pH 4.2) solutions irradiated (R-350) under N₂-sat conditions.

9. Fluorescence (EEMs) spectroscopic analysis of 2C solutions irradiated (LED-426) under different atmospheres

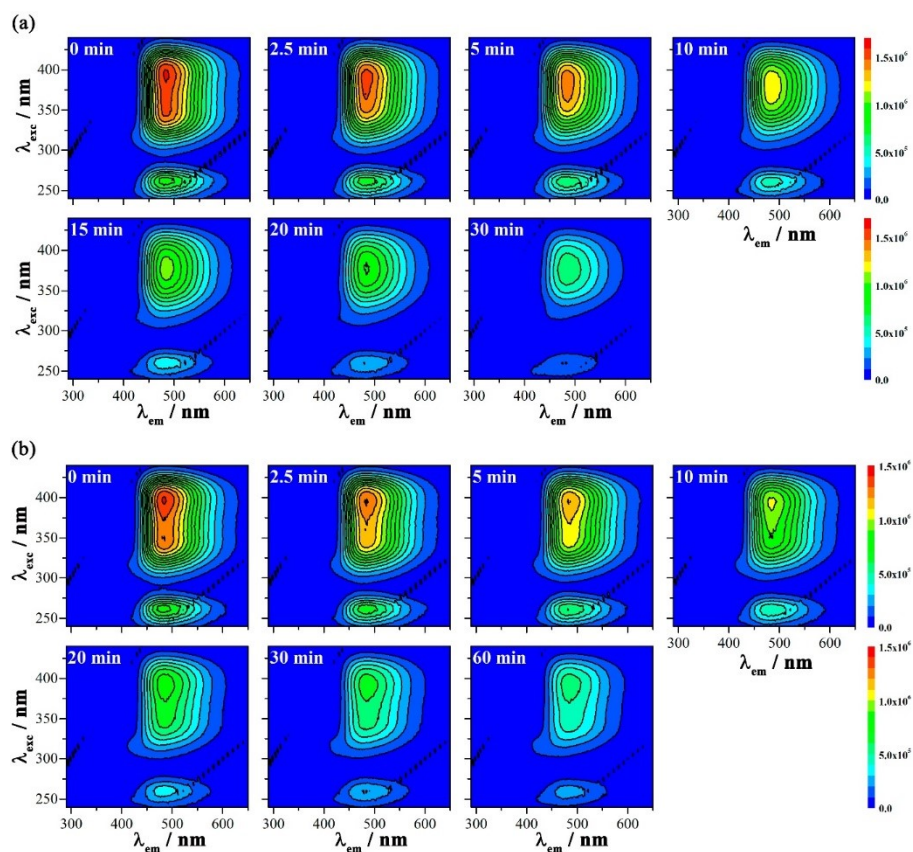


Figure SI.9. EEMs of 2C acidic (pH 4.2) solutions irradiated (LED-426) under (a) air-equilibrated and (b) N_2 -sat conditions.

10. UV-visible spectroscopic analysis of thermal reaction from 1C irradiated under different pH conditions

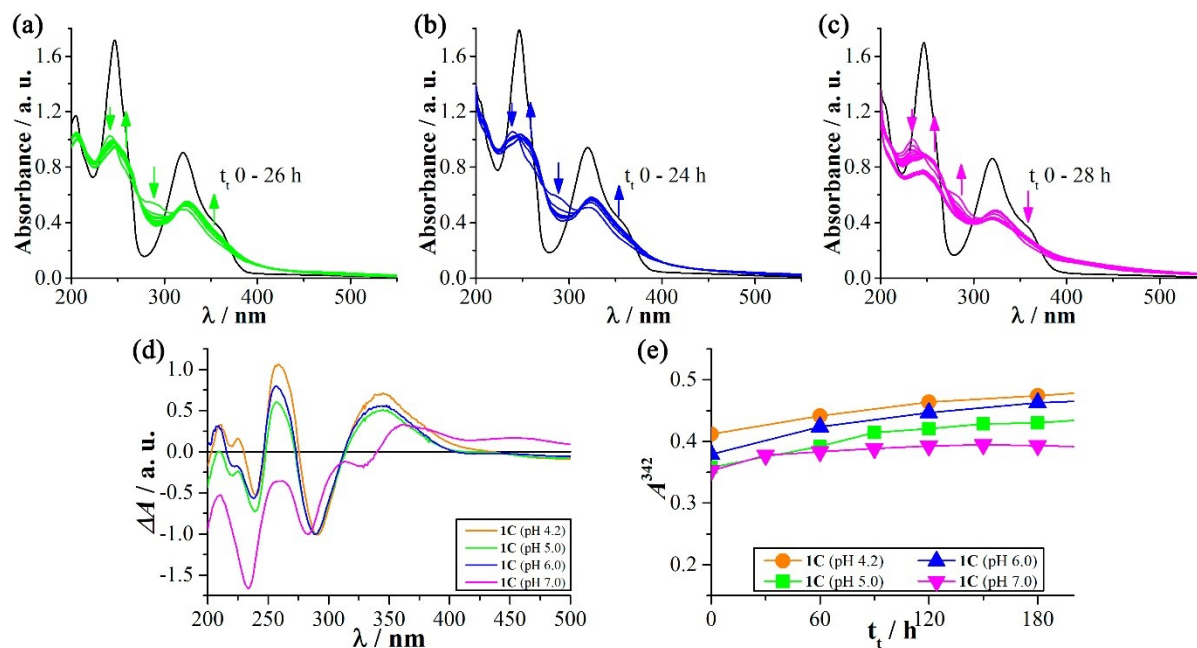


Figure SI.10. Evolution of the UV-visible spectra of the thermal reaction of the photoproducts formed upon irradiation (R-350, for 60 min) of 1C (50 μM) under air-equilibrated solutions at pH (a) 5.0 (green), (b) 6.0 (blue) and (c) 7.0 (pink). Measurements were made using quartz cells of 1 cm optical path lengths. For comparative purpose, black lines representing the absorption spectra of non-irradiated 1C solution are included. (d) and (e) NED_{ter} spectra and kinetics corresponding to data shown in (a) to (c). With comparative reasons, data presented in the main text corresponding to the pH 4.2 acidic condition are also depicted herein in orange.

11. UV-visible spectroscopic analysis of thermal reaction from 2C irradiated under different pH conditions

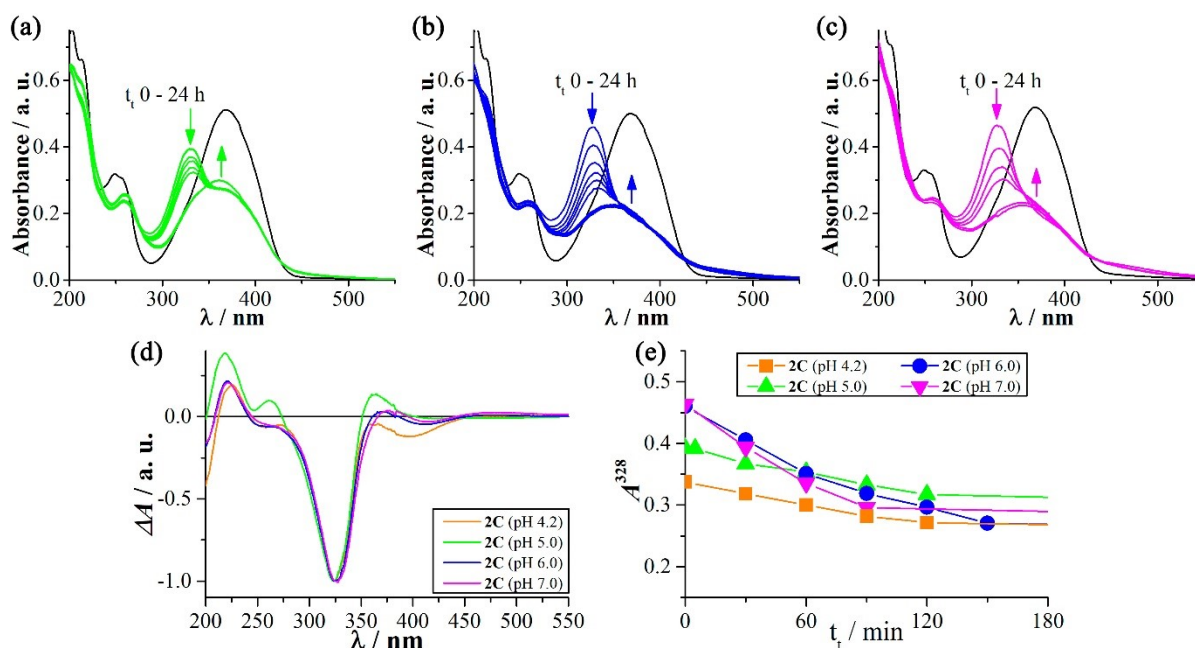


Figure SI.11. Evolution of the UV-visible spectra of the thermal reaction of the photoproducts formed upon irradiation (R-350, for 60 min) of air-equilibrated solution of 2C (32 μM) under various pH conditions: **(a)** 5.1 (green), **(b)** 6.0 (blue) and **(c)** 7.0 (pink). Measurements were made using quartz cells of 1 cm optical path lengths. For comparative purpose, black lines representing the absorption spectra of non-irradiated 1C solution are included. **(d)** and **(e)** NED_{ter} spectra and kinetics corresponding to data shown in (a) to (c). With comparative reasons, data presented in the main text corresponding to the pH 4.2 acidic condition are also depicted herein in orange.

12. UV-visible spectroscopic analysis of thermal reaction from 2C irradiated with LED-426

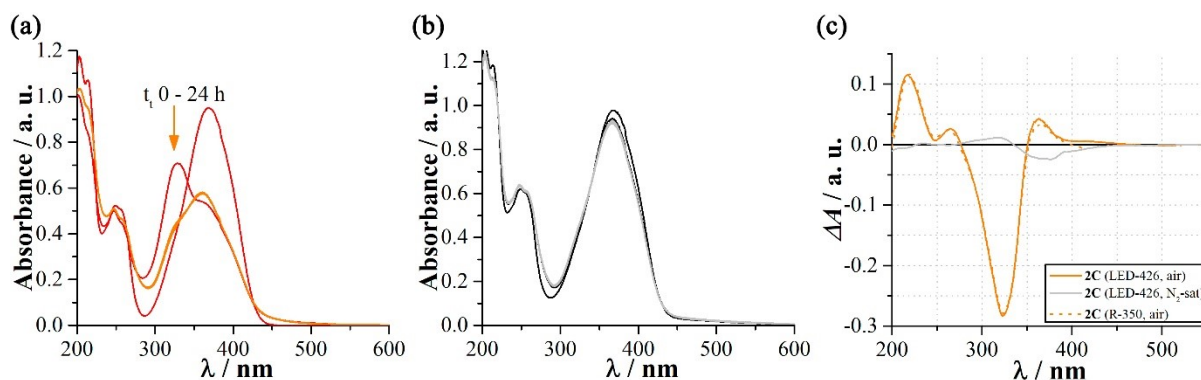


Figure SI.12. Evolution of the UV-visible spectra of the thermal reaction of the photoproducts formed upon irradiation (LED-426, for 35 min) of acidic (pH 4.2) aqueous solution of **2C** (60 μM) under (a) air-equilibrated and (b) N₂-sat atmospheric conditions. Measurements were made using quartz cells of 1 cm optical path lengths. For comparative purpose, the absorption spectrum of non-irradiated **2C** solution is included. (c) NED_{ter} spectra corresponding to data shown in (a) and (b) for the thermal reaction. NED_{ter} spectra were calculated by subtracting the spectra obtained after 24 h of dark incubation and the spectra recorded after 35 min of irradiation.

13. UV-visible spectroscopic analysis of the effect of oxygen on the thermal reaction of 2C photoproducts

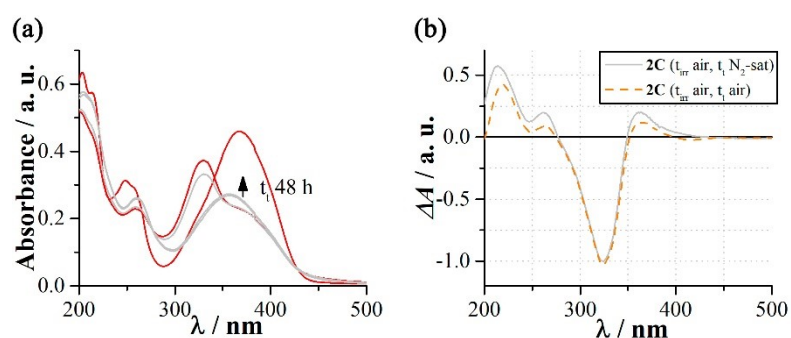


Figure SI.13. UV-visible spectra of the thermal reaction of the photoproducts formed upon irradiation (LED-426, for 35 min) of acidic (pH 4.2) aqueous solution of **2C** (30 μM) under air-equilibrated and storage under N_2 -sat conditions during 48 h. Measurements were made using quartz cells of 1 cm optical path lengths. For comparative purpose, the absorption spectra of non-irradiated (red solid line) and irradiated (R-350, for 60 min) solution are included. **(b)** NED_{ter} spectra corresponding to data shown in (a) for the thermal reaction. NED_{ter} spectra were calculated by subtracting the spectra obtained after 48 h of dark incubation under N_2 -sat and the spectra recorded after 60 min of irradiation. For comparative purpose, NED_{ter} spectrum corresponding to the thermal reaction performed under air-equilibrated conditions.

14. MCR-ALS analysis of 1C irradiated under different pH conditions

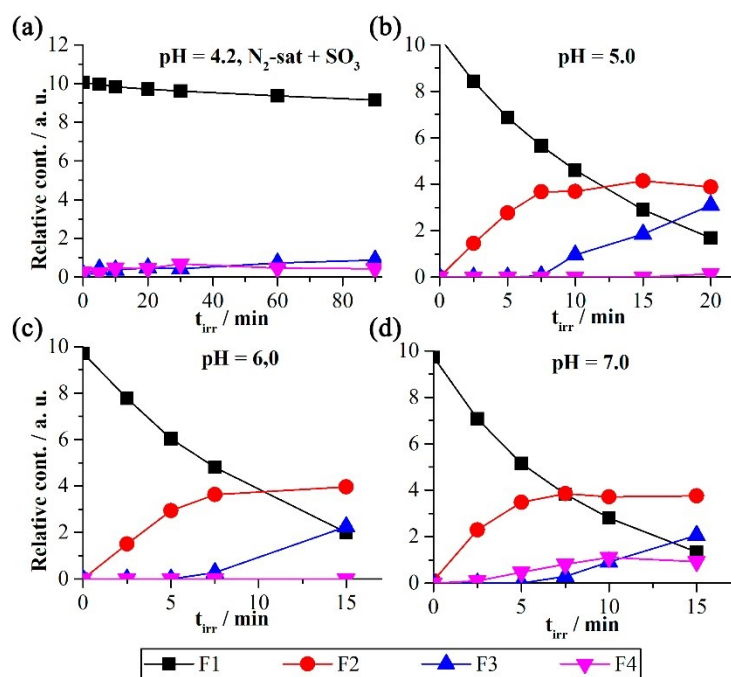


Figure SI.14. Kinetics profiles of factors F1 – F4 observed for the photochemical reaction (R-350) of **1C** performed under different experimental conditions (unimodality and non-negativity restrictions): (a) N₂-acidic (pH 4.2) solution. (b) air-equilibrated solution at pH 5.0. (c) air-equilibrated solution at pH 6.0. and (d) air-equilibrated solution at pH 7.0.

15. MCR-ALS analysis of 2C irradiated under different pH conditions

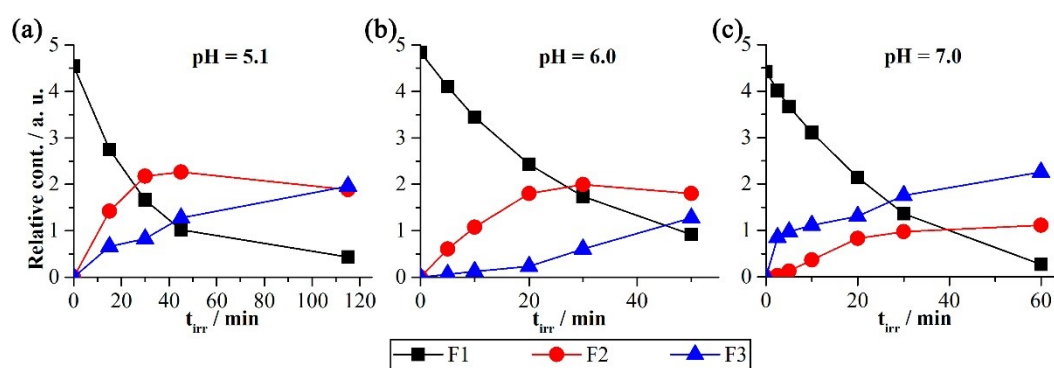


Figure SI.15. Kinetics profiles of factors F1 – F3 observed for the photochemical reaction (R-350) of 2C performed under air-equilibrated atmosphere at different pH conditions (unimodality and non-negativity restrictions): (a) pH 5.0. (b) pH 6.0. and (c) pH 7.0.

16. UV-visible spectroscopic titration of irradiated 1C solutions

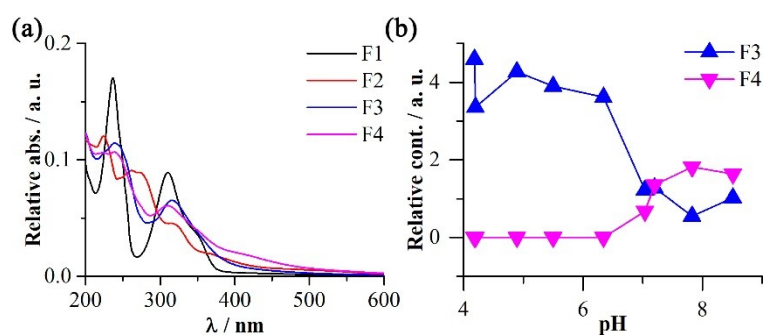


Figure SI.16. MCR-ALS analysis (unimodality and non-negativity restrictions) of the evolution of UV-visible absorption spectra of **1C** irradiated (R-350) solution under different pH conditions: **(a)** Spectroscopic profiles of factors F1 – F4. **(b)** Relative concentration (pseudo-titration curve) of F3 and F4 as a function of the pH.

17. MCR-ALS analysis of the thermal reaction of 1C and 2C irradiated solutions under different pHs

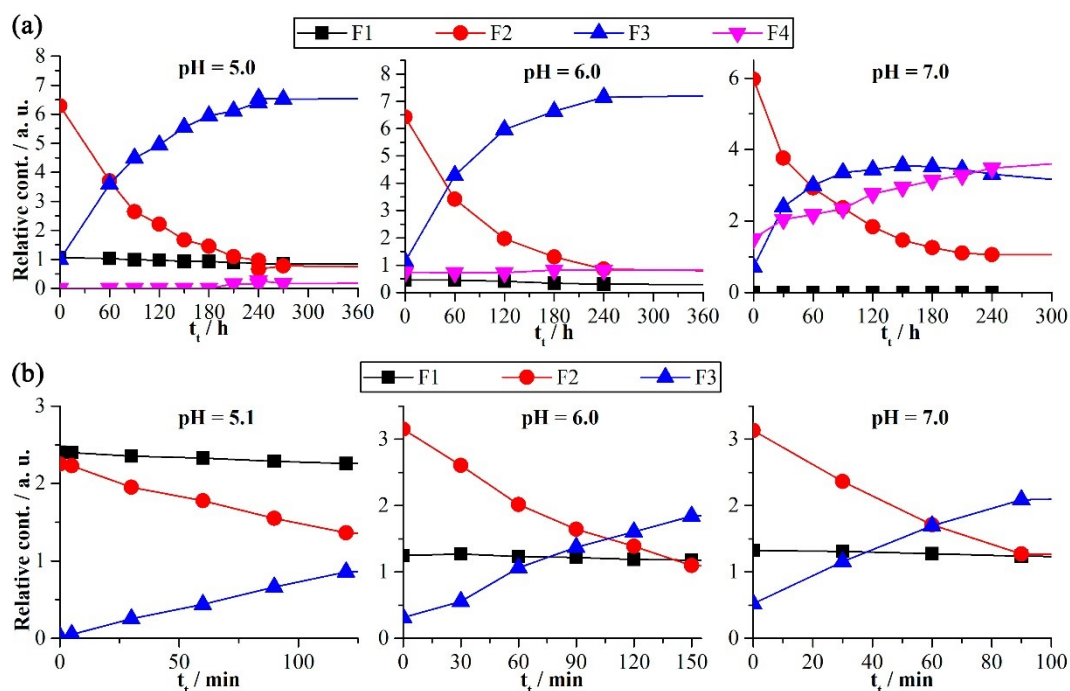


Figure SI.17. (a) and (b) Kinetics profiles of factors F1 – F4 observed for the photochemical reaction (R-350) of compounds 1C and 2C, respectively, performed under air-equilibrated atmosphere at different pH conditions (unimodality and non-negativity restrictions).

18. ESI analysis of relative intensities of 2C / 1C

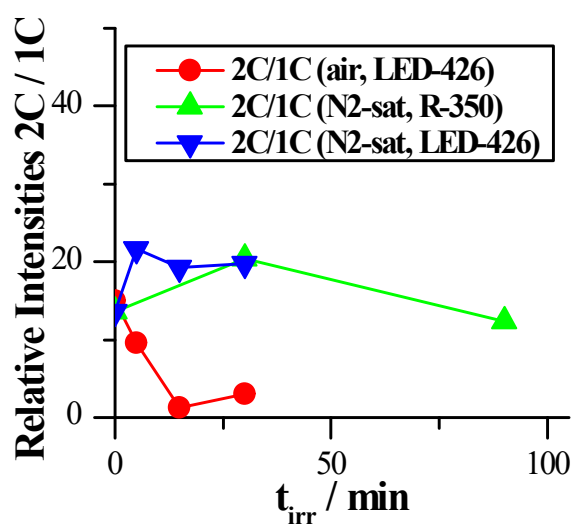


Figure SI.18. Pseudo-kinetics profiles of factors ESI intensities of **2C** relative to **1C** signal observed for the photochemical reaction (R-350 and LED-426) of compound **2C**, performed under air-equilibrated and N₂-sat atmospheres.

19. TD-DFT calculated electronic transitions and simulated spectra for the cationic (C) and quinonic (Q) species of compounds 1 and 2.

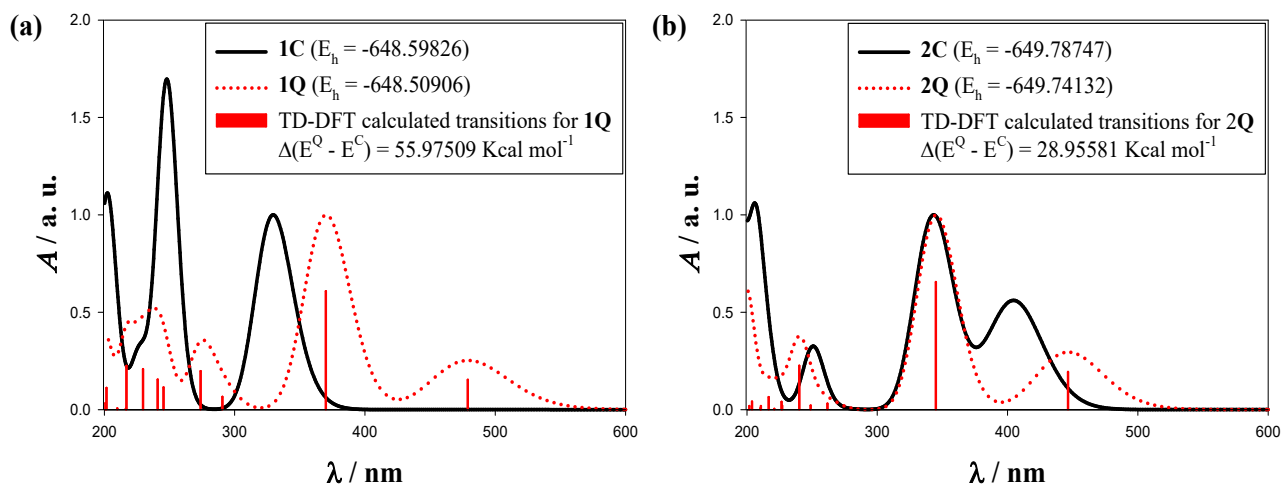


Figure SI.19. (a) and (b) Comparison of the TD-DFT calculated electronic transitions and simulated spectra for the cationic (C) and quinonic (Q) species of compounds **1** and **2**, respectively. The vertical transition energies were calculated at the optimized ground-state geometry by TD-DFT using B3LYP hybrid functional and aug-cc-pVDZ basis set including solvent effects (water) through the Polarizable Continuum Model. E_h is the SCF energy in Hartree.

20. Numerical support for H₂O₂ quantification

From **Figure 1b** it is evident that the slopes of the colorimetric reaction, evaluated in the absence and presence of catalase, show no significant difference. Therefore, there is a lack of H₂O₂ photoinduced formation. This observation suggests that, contrary to what has been well-documented for other related photoexcited βCs, compounds **1C** and **2C** follow a distinctive photochemical degradation pathway where dissolved molecular oxygen does not play a role as an electron acceptor to yield H₂O₂.

To further support this hypothesis, a numerical approach is provided herein to estimate a putative quantum yield of H₂O₂ formation ($\Phi_{\text{H}_2\text{O}_2}$) for comparison with the quantum yield of consumption of compounds **1C** and **2C** (Φ_{R} 83.0 × 10⁻³ and 20.3 × 10⁻³, respectively). To this aim, the corresponding calibration curve (**Figure SI.20**) for the colorimetric method used for H₂O₂ quantification was obtained, with a calibration factor of 0.00273 a.u. μM⁻¹.

Figure 1b shows the evolution of the absorbance at 505 nm as a function of the irradiation time ($A^{505\text{nm}}$ vs t_{irr}) for both untreated (CAT⁻) and treated irradiated samples (CAT⁺). Note that only for the case of **1C** a mild difference in the slopes was observed so it can be assumed that H₂O₂ production upon irradiation of **2C** is negligible. Moreover, for **1C** a negligible upper limit for the rate of H₂O₂ formation ($d[\text{H}_2\text{O}_2]/dt$) can be estimated from the difference between the two slopes (CAT⁻ - CAT⁺) and the corresponding H₂O₂ calibration factor (0.00273 a.u. μM⁻¹):

$$\Delta\text{slopes} = \text{CAT}^- - \text{CAT}^+ = (0.0019029 - 0.0014722) \text{ Abs}^{505} \text{ min}^{-1} = 4.3 \times 10^{-4} \text{ Abs}^{505} \text{ min}^{-1} \quad (1)$$

$$(d[\text{H}_2\text{O}_2]/dt) = 4.3 \times 10^{-4} \text{ Abs}^{505} \text{ min}^{-1} / 0.00273 \text{ a.u. } \mu\text{M}^{-1} = 0.15 \mu\text{M min}^{-1} \quad (2)$$

Considering the photon flux ($P_0 = 7.0 \times 10^{-5} \text{ E min}^{-1}$) as well as the absorbance at the excitation wavelength 350 nm ($A^{350\text{nm}} = 0.4$), an upper limit for the corresponding quantum yield of H₂O₂ production by **1C** can be estimated:

$$\Phi_{\text{H}_2\text{O}_2} = (d[\text{H}_2\text{O}_2]/dt) / P_0 (1 - 10^{-A^{350}}) = 0.15 \times 10^{-6} \text{ M min}^{-1} / (7.0 \times 10^{-5} \text{ E min}^{-1} (1 - 10^{-0.4})) = 3.6 \times 10^{-3} \quad (2)$$

The upper limit estimated for H₂O₂ formation ($\Phi_{\text{H}_2\text{O}_2} = 3.6 \times 10^{-3}$) is one order of magnitude lower than the corresponding quantum yield of **1C** consumption ($\Phi_{\text{R}} = 83.0 \times 10^{-3}$). This large difference confirms that also **1C** follows a distinctive photochemical mechanism, which is independent of H₂O₂ production.

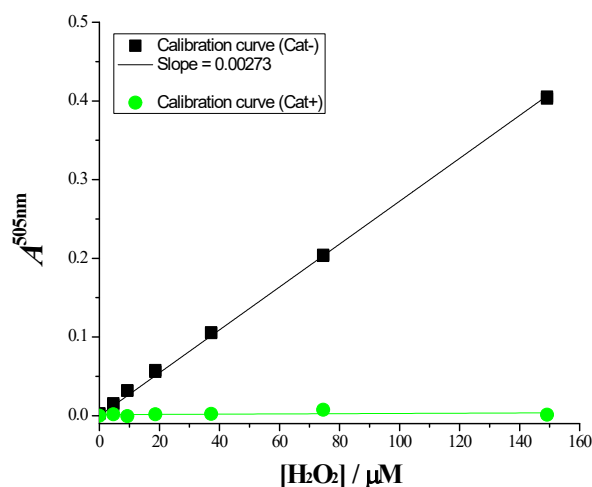


Figure SI.20. Calibration curve for H₂O₂ quantification. Black and green symbols correspond to the catalase untreated (CAT⁻) and pretreated (CAT⁺) samples. Aqueous H₂O₂ solutions prepared from commercial standards were employed for obtaining the corresponding calibration curves.[36]